Optimal Power Management of Battery Energy Storage Systems via Ensemble Kalman Inversion

Amir Farakhor[1], Iman Askari[1], Di Wu[2], and Huazhen Fang[1]

***Abstract*— Optimal power management of battery energy storage systems (BESS) is crucial for their safe and efficient operation. Numerical optimization techniques are frequently utilized to solve the optimal power management problems. However, these techniques often fall short of delivering real-time solutions for large-scale BESS due to their computational complexity. To address this issue, this paper proposes a computationally efficient approach. We introduce a new set of decision variables called *power-sharing ratios* corresponding to each cell, indicating their allocated power share from the output power demand. We then formulate an optimal power management problem to minimize the system-wide power losses while ensuring compliance with safety, balancing, and power supply-demand match constraints. To efficiently solve this problem, a parameterized control policy is designed and leveraged to transform the optimal power management problem into a parameter estimation problem. We then implement the ensemble Kalman inversion to estimate the optimal parameter set. The proposed approach significantly reduces computational requirements due to 1) the much lower dimensionality of the decision parameters and 2) the estimation treatment of the optimal power management problem. Finally, we conduct extensive simulations to validate the effectiveness of the proposed approach. The results show promise in accuracy and computation time compared with explored numerical optimization techniques.**

I. Introduction

Battery energy storage systems (BESS) have found widespread use in various applications ranging from small portable electronics to large-scale battery packs for electric vehicles and grid energy storage [1, 2]. These BESS comprise many battery cells connected in series/parallel to deliver the required output voltage/capacity requirements. BESS power management commonly refers to power distribution among these constituent cells for the sake of multiple operational objectives. Conventional power management strategies mainly focus on state-of-charge (SoC) balancing to maximize the BESS utilization [3]. However, recent studies have pointed out further potentials that lie in optimal power management, including temperature balancing and output voltage regulation [4]. Despite the evident advantages of optimal power management, its practical implementation presents a nontrivial challenge. The underlying optimization problem can quickly reach a formidable level of computational complexity with an increasing number of cells, rendering real-time execution infeasible. While different strategies have been explored in the literature to alleviate computational requirements, optimal power management remains hardly attainable for large-scale BESS. In this paper, we propose a novel perspective on optimal power management, leveraging Bayesian estimation to significantly reduce computation. Next, we will review the existing literature on optimal power management.

A. Literature Review

Optimal power management brings about several key operational features, including power loss minimization, cell balancing, and charge/discharge control. To fully harness these functionalities, the literature has devised various optimization problems. Conventionally, the focus has centered around SoC balancing to maximize the BESS utilization. For instance, the study in [5] introduces a linear program aimed at achieving SoC balancing either in minimum time or with minimum power loss. This work is subsequently expanded in [6] to enable inter- and intra-module level SoC balancing. Further, in [7], a convex optimization problem is formulated to achieve multiple objectives of cell balancing and power loss minimization. Building upon this work, the studies in [8, 9] extend this formulation to accommodate other BESS configurations. We have also tailored a convex optimization problem for a reconfigurable BESS in our previous study [10]. The study in [11] also formulates a hierarchical model predictive control for optimal power management.

In hindsight, optimal power management approaches leverage the power of their underlying optimization problems to enhance BESS performance. These problems are typically solved through computationally intensive numerical techniques. However, computational demands of these methods become enormous when large-scale BESS presents large numbers of decision variables, thus hindering the practical implementation.

Distributed control is a valuable approach to managing large-scale systems. This method involves distributing control tasks and computations among the constituent units or agents of the system. This approach provides improved efficiency and scalability, making it a useful choice for BESS power control. Recent studies in [12, 13] treat individual cells as autonomous agents and employed the concept of distributed average consensus within networked multi-agent

[1]A. Farakhor, I. Askari and H. Fang are with the Department of Mechanical Engineering, University of Kansas, Lawrence, KS, USA. Email: {a.farakhor, askari, fang}@ku.edu

[2]D. Wu is with the Pacific Northwest National Laboratory, Richland, WA, USA. Email: di.wu@pnnl.gov

systems to develop algorithms for SoC balancing. However, these methods have limitations in optimizing critical metrics such as power losses, making them non-optimal. Our previous research in [14] also proposes an innovative distributed optimal power management approach that is specifically designed for large-scale BESS.

B. Summary of Contributions

Despite efforts to reduce computational complexity, optimal power management for large-scale BESS applications still remains beyond the reach of existing methods. Towards overcoming the situation, our paper delivers the following contributions:

1) We introduce power-sharing ratios for the cells which indicate their power quota from the demanded output power. This facilitates formulating an optimal power management problem, leading to two benefits: firstly, the optimal power-sharing ratios depend solely on current cell conditions such as SoC, temperature, and internal resistance. This allows us to propose a parameterized control policy to reduce the number of decision variables remarkably. Secondly, it streamlines the Bayesian estimation treatment of the optimal power management problem by limiting the search space of control variables.
2) We formulate and convert an optimal power management problem into a Bayesian parameter estimation problem. Avoiding tedious numerical optimization, we instead perform estimation to enable optimal power management. We specifically leverage ensemble Kalman inversion to estimate the optimal parameter set for the proposed control policy. The estimation framework substantially reduces computation time, making optimal power management potentially feasible and scalable for real-world applications.

We validate our approach through extensive simulations, demonstrating its efficacy in terms of accuracy and computation time.

II. Optimal Power Management of BESS

This section elaborates on the BESS circuit structure, its electro-thermal modeling, and optimal power management formulation.

A. Circuit Structure

Fig. 1 illustrates the circuit structure of the considered BESS. It comprises n battery cells. Each cell is equipped with its corresponding DC/DC converter, which can be interconnected in series or parallel configurations to supply the load under specific voltage/capacity ratings. The DC/DC converters allow bidirectional power processing to charge/discharge the cells with regulated power. This brings about cell-level power control for the considered BESS. This paper leverages this feature to enable cell balancing and power loss minimization. It is worth mentioning that

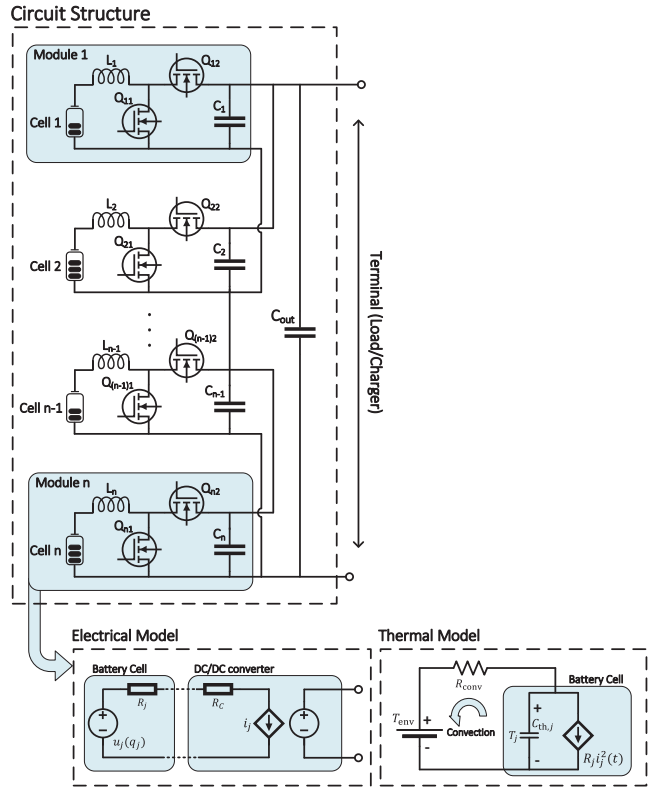

Fig. 1: The circuit structure of large-scale BESS.

the proposed approach in this work extends to other circuit structures capable of cell-level power control. The following subsection provides an electro-thermal model for the BESS to pave the path for the problem formulation.

B. Electro-thermal Modeling

We begin by characterizing the electrical dynamics of the considered BESS. Each cell is described by the Rint model, which encompasses a SoC-dependent open-circuit voltage (OCV) and a series resistance [15]. Further, we model the DC/DC converters using an ideal DC transform and a series resistance to capture their inherent inefficiencies. The electrical model is illustrated in Fig. 1. For cell j, the governing equations are given by

$$\dot{q}_j(t) = -\frac{1}{Q_j} i_j(t), \tag{1a}$$

$$v_j(t) = u_j(q_j(t)) - R_j i_j(t), \tag{1b}$$

where v_j, u_j, R_j, i_j, Q_j, q_j are the terminal voltage, OCV, internal resistance, current, capacity, and SoC, respectively. The cell's internal charging/discharging power P_{b_j} is defined as follows:

$$P_{b_j} = u_j(q_j(t)) i_j(t). \tag{2}$$

Further, the cell's and its corresponding converter's power losses are expressed by

$$P_{L_j} = (R_j + R_C) i_j^2(t). \tag{3}$$

For the cells, let us introduce the power-sharing ratios. This quantity indicates the portion of power allocated to each cell from the total output power demand. They are defined as

$$\mu_j = \frac{P_{b_j}}{|P_{\text{out}}|}, \tag{4}$$

where μ_j and P_{out} are the power-sharing ratio and output power demand, respectively. Note that we consider the absolute value of P_{out} in (4) to accommodate both charging and discharging cycles. Proceeding forward, we rewrite (1a) and (3) to represent them in terms of μ_j. The new expressions are as follows:

$$\dot{q}_j(t) = -\frac{\mu_j(t)P_{\text{out}}(t)}{Q_j u_j(q_j(t))}, \tag{5a}$$

$$P_{L_j} = \frac{(R_j + R_C)\mu_j^2(t)P_{\text{out}}^2(t)}{u_j^2(q_j(t))}. \tag{5b}$$

Next, we describe the cells' thermal behavior using a lumped thermal circuit. The temperature of the cells is influenced by heat generation due to internal power losses, and heat dissipation due to environmental convection. For cell j, the governing dynamic equation is

$$C_{\text{th},j}\dot{T}_j(t) = \frac{R_j\mu_j^2 P_{\text{out}}^2(t)}{u_j^2(q_j(t))} - (T_j(t) - T_{\text{env}})/R_{\text{conv}}, \tag{6}$$

where $C_{\text{th},j}$, T_j, T_{env}, and R_{conv} are the thermal capacitance, cell's temperature, environmental temperature, and convective thermal resistance, respectively. The collective electro-thermal model, described in (5) and (6), strikes an appropriate balance between expressiveness and computational tractability to pave the path toward optimal power management formulation.

C. Problem Formulation

Here, we introduce the proposed optimal power management approach based on the power-sharing ratios. The main objective of our approach is to achieve a power-loss-minimized BESS operation while adhering to safety, balancing, and power supply-demand match requirements. The formulation in the sequel is represented in discrete time after discretizing the electro-thermal model via the forward Euler method.

To begin with, we express the BESS power losses at time instant t as follows:

$$J[t] = \sum_{j=1}^{n} \frac{(R_j + R_C)\mu_j^2[t]P_{\text{out}}^2[t]}{u_j^2(q_j[t])}. \tag{7}$$

To ensure the safe operation of the BESS, we impose the following constraints:

$$i_j^{\min} \le i_j \le i_j^{\max}, \tag{8a}$$

$$q_j^{\min} \le q_j \le q_j^{\max}, \tag{8b}$$

where $i_j^{\min/\max}$ and $q_j^{\min/\max}$ are the lower/upper safety bounds for the cells' current and SoC. Note that we can express (8a) in terms of the power-sharing ratios as follows:

$$\frac{u_j(q_j[t])}{\left|P_{\text{out}}[t]\right|} i_j^{\min} \le \mu_j[t] \le \frac{u_j(q_j[t])}{\left|P_{\text{out}}[t]\right|} i_j^{\max}. \tag{9}$$

To promote balanced cell use, we further enforce constraints on BESS operation as follows:

$$\left|q_j[t] - q_{\text{avg}}[t]\right| \le \Delta q, \tag{10a}$$

$$\left|T_j[t] - T_{\text{avg}}[t]\right| \le \Delta T, \tag{10b}$$

where $q_{\text{avg}}[t]$ and $T_{\text{avg}}[t]$ represent the average SoC and temperature, and Δq and ΔT are the allowed deviation of the cells' SoC and temperature from their respective average values. The power supply-demand balance can also be guaranteed using the following constraint:

$$\sum_{j=1}^{n}\left(\mu_j[t] - \frac{(R_j + R_C)\mu_j^2[t]\left|P_{\text{out}}[t]\right|}{u_j^2(q_j[t])}\right) = 1. \tag{11}$$

Having laid out the power loss expression and the constraints, we can now proceed to formulate the optimal power management problem over a receding horizon as follows:

$$\begin{aligned} \min_{\mu_j, j=1,\ldots,n} \quad & \sum_{t=k}^{k+H} J[t], \\ \text{s.t.} \quad & (5a), (6), (8b), (9), (10), (11), \end{aligned} \tag{12}$$

where H is the horizon length. Note that the optimization problem stated in (12) is both non-linear and non-convex, and requires optimization of $3nH - n$ variables. While it may be feasible to manage its computation for small n, it can quickly become extremely challenging for large-scale BESS. Therefore, we aim to develop a computationally efficient solution for (12) in the next section.

III. Efficient Optimal Power Management Approach

This section introduces a parameterized control policy for the optimal power management problem and then translates it into a Bayesian parameter estimation problem. Finally, we leverage the ensemble Kalman inversion for parameter estimation.

A. Input Parameterization

As previously discussed, the computational complexity of (12) hinders the adoption of optimal power management for large-scale BESS. To alleviate this issue, we propose a parameterized control policy based on the BESS operational conditions. By doing so, we intend to map a high-dimensional control space, power-sharing ratios, into a low-dimensional parameter space. Before introducing the control policy, we explain the rationale behind this design with an example. Let us consider a BESS with uniform SoC distribution except for one cell with a relatively lower SoC value. To achieve a balance, we require this cell to be allocated more/less power in charging/discharging cycles. We

also need analogous behavior for the cells' temperatures and internal resistances. We thus parameterize the control policy as follows to generate such behaviors:

$$\mu_j[k] = \begin{bmatrix}\theta_1 & \theta_2 & 1-\theta_1-\theta_2\end{bmatrix}^\top \begin{bmatrix} l_{q,j} \\ l_{T,j} \\ l_{R,j}\end{bmatrix}, \tag{13}$$

where θ_1 and θ_2 are the parameters; $l_{q,j}$, $l_{T,j}$, and $l_{R,j}$ are also defined as follows:

$$l_{q,j} = \begin{cases} \sum_{i=1}^n \left(\frac{q_j}{q_i}\right)^{-\beta_1} & P_{\text{out}} \geq 0 \\ \sum_{i=1}^n \left(\frac{q_i}{q_j}\right)^{-\beta_1} & P_{\text{out}} < 0 \end{cases}, \tag{14a}$$

$$l_{T,j} = \sum_{i=1}^n \left(\frac{T_j}{T_i}\right)^{-\beta_2}, \tag{14b}$$

$$l_{R,j} = \left(\sum_{i=1}^n \frac{R_j}{R_i}\right)^{-1}, \tag{14c}$$

where β_1 and β_2 are the hyperparameters. These hyperparameters play a crucial role in the SoC and temperature balancing performance, as they amplify the impact of imbalance on the power-sharing ratios. Specifically, higher values of β lead to greater differentiation in power allocation among the cells. One can select β_1 and β_2 based on BESS specifications.

Remark 1. *The control policy proposed in* (13) *maintains optimality regarding power loss minimization. This is because* (14c) *is indeed the solution of* (12) *when the safety and balancing constraints* (8b)*,* (9)*, and* (10) *are not active. By setting* $\theta_1 = \theta_2 = 0$*, the designed control policy reflects the absence of balancing constraints. Thus, the resultant power-sharing ratios achieve power-loss-minimizing operation.*

With the above control policy parameterization, the number of optimization variables reduce to $2nH + 2$, in contrast to $3nH - n$ in the original problem. We will make further effort next to find out the best optimization variables with fast computation.

B. Bayesian Estimation Formulation

We leverage the designed control policy in (13) to translate (12) into a Bayesian parameter estimation problem. The estimation framework centers around utilizing the cost function (power losses) and the constraints (safety, balancing, and power conservation) to collectively guide the inference of optimal parameter set. The primary objective of this transformation is twofold. Firstly, it provides us access to sophisticated tools developed in the field of estimation. Secondly, it leads to a significant reduction in computation. We begin the transformation by introducing a virtual dynamic system. While doing so, we use simplified notations for compact representations and adopt the convention of using boldface lowercase letters for vectors and boldface uppercase letters for matrices. The virtual dynamics are expressed as follows:

$$\begin{cases} \boldsymbol{x}[t+1] = \boldsymbol{f}\big(\boldsymbol{x}[t], \boldsymbol{\pi}_{\boldsymbol{\theta}}(\boldsymbol{x}[t])\big), \\ y[t] = h\big(\boldsymbol{x}[t], \boldsymbol{\pi}_{\boldsymbol{\theta}}(\boldsymbol{x}[t])\big) + v[t], \end{cases} \tag{15}$$

where $\boldsymbol{x}[t]$, $\boldsymbol{\mu}[t]$, and $\boldsymbol{\theta}$ collect the cells' SoC and temperature values, power-sharing ratios, and parameters as follows:

$$\begin{aligned} \boldsymbol{x}[t] &= \begin{bmatrix} q_1[t] & \dots & q_n[t] & T_1[t] & \dots & T_n[t]\end{bmatrix}^\top, \\ \boldsymbol{\mu}[t] &= \begin{bmatrix}\mu_1[t] & \dots & \mu_n[t]\end{bmatrix}^\top, \\ \boldsymbol{\theta} &= \begin{bmatrix}\theta_1 & \theta_2 & 1-\theta_1-\theta_2\end{bmatrix}^\top. \end{aligned}$$

Further, $\boldsymbol{f}$ denotes the discretized dynamic equations in (5a) and (6) for all cells; $\boldsymbol{\mu}[t] = \boldsymbol{\pi}_{\boldsymbol{\theta}}(\boldsymbol{x}[t])$ represents the parameterized control policy in (13). The virtual measurement $y[t]$ is characterized by

$$h\big(\boldsymbol{x}[t], \boldsymbol{\pi}_{\boldsymbol{\theta}}(\boldsymbol{x}[t])\big) = J[t] + \psi\big(g\left(\boldsymbol{x}[t], \boldsymbol{\pi}_{\boldsymbol{\theta}}(\boldsymbol{x}[t])\right)\big), \tag{16}$$

where $g[t]$ gathers the constraints in (8b), (9), (10), (11) for all cells at time t. Also, $\psi(\cdot)$ is a barrier function to measure the constraint satisfaction as follows:

$$\psi(x) = \begin{cases} 0 & x \leq 0 \\ \infty & x > 0 \end{cases}. \tag{17}$$

In this framework, we relax the virtual measurement $y[t]$ to be stochastic by introducing a random noise variable $v[t]$.

We highlight that the virtual system replicates the dynamics of the original system as in (12). The only difference is that the hard constraints in (12) are relaxed to a soft constraint and added as a penalty term in the virtual measurements. Furthermore, it is crucial for the behavior of virtual measurements to mirror the characteristics of the optimization problem in (12). This necessitates that the virtual measurements conform to the form where $y[t] = 0$ holds for $t = k, \dots, k+H$. Requiring $y[t] = 0$ drives the BESS operation close to the ideal case characterized by negligible power losses and constraint satisfaction.

We are now ready to perform parameter estimation given the virtual dynamics in (15). This involves the consideration of the posterior distribution $p(\boldsymbol{\theta} \,|\, \boldsymbol{y} = \boldsymbol{0})$ with the concatenated measurements from $t = k, \dots, k+H$, i.e.,

$$\boldsymbol{y} = \begin{bmatrix} y[k] & \dots & y[k+H]\end{bmatrix}^\top.$$

To estimate $\boldsymbol{\theta}$, we apply the maximum a posteriori (MAP) estimation:

$$\hat{\boldsymbol{\theta}}^* = \arg\max_{\boldsymbol{\theta}} \ \log p(\boldsymbol{\theta} \,|\, \boldsymbol{y} = \boldsymbol{0}). \tag{18}$$

Theorem 1. *Assume that* $p(\boldsymbol{\theta}) \sim \mathcal{N}(\bar{\boldsymbol{\theta}}, \boldsymbol{\Sigma}^{\boldsymbol{\theta}})$ *and that* $p(v) \sim \mathcal{N}(0, R)$ *in* (15) *is white noise. Then, the problems in* (12) *and* (18) *share the same optima when* $\boldsymbol{\theta}$ *has a noninformative prior, i.e.,* $\boldsymbol{\Sigma}^{\boldsymbol{\theta}} \to \infty$.

Proof. Using the Bayes' rule and the Markovian property of

(15), we have

$$p(\boldsymbol{\theta} \,|\, \boldsymbol{y} = \mathbf{0}) \propto \prod_{t=k}^{k+H} p(y[t] = 0 \,|\, \boldsymbol{\theta}) p(\boldsymbol{\theta}),$$

which implies

$$\log p(\boldsymbol{\theta} \,|\, \boldsymbol{y} = \mathbf{0}) = \sum_{t=k}^{k+H} \log p(y[t] = 0 \,|\, \boldsymbol{\theta}) + \log p(\boldsymbol{\theta}).$$

Because $p(y[t] = 0 \,|\, \boldsymbol{\theta}) \propto p(v[t]) \sim \mathcal{N}(0, R)$, we get

$$\log p(y[t] = 0 \,|\, \boldsymbol{\theta}) \propto \frac{1}{R} h^2 \left(\boldsymbol{x}[t], \boldsymbol{\pi}_{\boldsymbol{\theta}}(\boldsymbol{x}[t]) \right).$$

Further, $\log p(\boldsymbol{\theta}) \to 0$ as $\boldsymbol{\Sigma}^{\boldsymbol{\theta}} \to \infty$. Putting together the above, we see that the cost function in (18) is the scaled opposite of the cost function and soft constraints in (12). The theorem is thus proven. □

Theorem 1 suggests the equivalence between the estimation problem in (18) and the problem in (12) under mild conditions. However, finding an analytical solution to (18) is not possible, so we develop approximate solutions to (18). It is important to note that the noninformative prior assumption for $p(\boldsymbol{\theta})$ in Theorem 1 implies that the initial prior covariance should be large enough to enable the exploration of the entire search space. Next, we employ the ensemble Kalman inversion to approximately solve (18).

C. Parameter Estimation via Ensemble Kalman Inversion

Tracing to ensemble Kalman filtering, the ensemble Kalman inversion method enables sampling-based approximation of a target posterior distribution [16]. It is effective in finding the unknown parameters of a complex system given measurement data. Its computation is derivative-free and fast by harnessing the power of sampling. Specifically, the method iteratively approximates $p(\boldsymbol{\theta}_{\ell+1} \mid \boldsymbol{y})$ through

$$p(\boldsymbol{\theta}_{\ell+1} \,|\, \boldsymbol{y}) \propto p(\boldsymbol{y} \,|\, \boldsymbol{\theta}_\ell)^{\alpha_\ell} p(\boldsymbol{\theta}_\ell), \tag{19}$$

where ℓ is the iteration index and $0 \leq \alpha_\ell \leq 1$ is a varying hyperparameter used to temper the likelihood. As will be seen later, α_ℓ will play the role of a stepsize parameter in the sampling-based update procedure [17]. We consider that $p(\boldsymbol{\theta}_\ell) \sim \mathcal{N}(\bar{\boldsymbol{\theta}}_\ell, \boldsymbol{\Sigma}_l^{\boldsymbol{\theta}})$. Note that $p(\boldsymbol{y} \,|\, \boldsymbol{\theta}_\ell)^{\alpha_\ell}$ has covariance $\alpha_\ell^{-1} \boldsymbol{R}$, where $\boldsymbol{R} = \mathrm{diag}(R, \ldots, R)$. We assume

$$p\left(\begin{bmatrix} \boldsymbol{\theta}_\ell \\ \boldsymbol{y} \end{bmatrix} \right) \sim \mathcal{N}\left(\begin{bmatrix} \bar{\boldsymbol{\theta}}_\ell \\ \bar{\boldsymbol{y}}_\ell \end{bmatrix}, \begin{bmatrix} \boldsymbol{\Sigma}_\ell^{\boldsymbol{\theta}} & \boldsymbol{\Sigma}_\ell^{\boldsymbol{\theta y}} \\ \left(\boldsymbol{\Sigma}_\ell^{\boldsymbol{\theta y}}\right)^\top & \boldsymbol{\Sigma}_\ell^{\boldsymbol{y}} + \alpha_\ell{}^{-1} \boldsymbol{R} \end{bmatrix} \right). \tag{20}$$

It follows from (20) that

$$p(\boldsymbol{\theta}_{\ell+1} \,|\, \boldsymbol{y}) \sim \mathcal{N}\left(\bar{\boldsymbol{\theta}}_{\ell+1}, \boldsymbol{\Sigma}_{\ell+1}^{\boldsymbol{\theta}} \right), \tag{21}$$

where

$$\bar{\boldsymbol{\theta}}_{\ell+1} = \bar{\boldsymbol{\theta}}_\ell + \boldsymbol{\Sigma}_\ell^{\boldsymbol{\theta y}} \left(\boldsymbol{\Sigma}_\ell^{\boldsymbol{y}} + \alpha_\ell{}^{-1} \boldsymbol{R} \right)^{-1} \left(\boldsymbol{y} - \bar{\boldsymbol{y}}_\ell \right), \tag{22a}$$

$$\boldsymbol{\Sigma}_{\ell+1}^{\boldsymbol{\theta}} = \boldsymbol{\Sigma}_\ell^{\boldsymbol{\theta}} + \boldsymbol{\Sigma}_\ell^{\boldsymbol{\theta y}} \left(\boldsymbol{\Sigma}_\ell^{\boldsymbol{y}} + \alpha_\ell{}^{-1} \boldsymbol{R} \right)^{-1} \left(\boldsymbol{\Sigma}_\ell^{\boldsymbol{\theta y}} \right)^\top. \tag{22b}$$

Based on (21)-(22), we can perform sampling-based approximation and update the posterior distribution. At iteration ℓ, we have $\boldsymbol{\theta}_\ell^{(i)} \sim \mathcal{N}(\boldsymbol{\theta}_\ell, \boldsymbol{\Sigma}_l^{\boldsymbol{\theta}})$ for $i = 1, \ldots, N$, and then generate the sampled trajectories for the state for $k \leq t \leq k + H$ by

$$\boldsymbol{x}_\ell^{(i)}[t+1] = \boldsymbol{f}\left(\boldsymbol{x}_\ell^{(i)}[t], \boldsymbol{\pi}_{\boldsymbol{\theta}_\ell^{(i)}}(\boldsymbol{x}_\ell^{(i)}[t]) \right), \quad i = 1, \ldots, N. \tag{23}$$

Then, the samples to approximate $p(\boldsymbol{y} \,|\, \boldsymbol{\theta}_\ell)$ can be computed by

$$y_\ell^{(i)}[t] = h\left(\boldsymbol{x}_\ell^{(i)}[t], \boldsymbol{\pi}_{\boldsymbol{\theta}_\ell^{(i)}}(\boldsymbol{x}_\ell^{(i)}[t]) \right) + v_\ell^{(i)}[t], \tag{24}$$

where $v_\ell^{(i)}[t] \sim \mathcal{N}(0, R)$. We now can calculate the means and covariances as below:

$$\bar{\boldsymbol{\theta}}_\ell = \frac{1}{N} \sum_{i=1}^{N} \boldsymbol{\theta}_\ell^{(i)}, \quad \bar{\boldsymbol{y}}_\ell = \frac{1}{N} \sum_{i=1}^{N} \boldsymbol{y}_\ell^{(i)}, \tag{25a}$$

$$\boldsymbol{\Sigma}_\ell^{\boldsymbol{\theta}} = \frac{1}{N-1} \sum_{i=1}^{N} \left(\boldsymbol{\theta}_\ell^{(i)} - \bar{\boldsymbol{\theta}}_\ell \right) \left(\boldsymbol{\theta}_\ell^{(i)} - \bar{\boldsymbol{\theta}}_\ell \right)^\top, \tag{25b}$$

$$\boldsymbol{\Sigma}_\ell^{\boldsymbol{y}} = \frac{1}{N-1} \sum_{i=1}^{N} \left(\boldsymbol{y}_\ell^{(i)} - \bar{\boldsymbol{y}}_\ell \right) \left(\boldsymbol{y}_\ell^{(i)} - \bar{\boldsymbol{y}}_\ell \right)^\top, \tag{25c}$$

$$\boldsymbol{\Sigma}_\ell^{\boldsymbol{\theta y}} = \frac{1}{N-1} \sum_{i=1}^{N} \left(\boldsymbol{\theta}_\ell^{(i)} - \bar{\boldsymbol{\theta}}_\ell \right) \left(\boldsymbol{y}_\ell^{(i)} - \bar{\boldsymbol{y}}_\ell \right)^\top. \tag{25d}$$

By (22a), the samples to approximate $p(\boldsymbol{\theta}_{\ell+1} \,|\, \boldsymbol{y})$ are

$$\boldsymbol{\theta}_{\ell+1}^{(i)} = \boldsymbol{\theta}_\ell^{(i)} + \boldsymbol{\Sigma}_\ell^{\boldsymbol{\theta y}} \left(\boldsymbol{\Sigma}_\ell^{\boldsymbol{y}} + \alpha_\ell{}^{-1} \boldsymbol{R} \right)^{-1} \left(\boldsymbol{y} - \boldsymbol{y}_\ell^{(i)} \right). \tag{26}$$

Generally, α_ℓ takes a small value in early iterations, and increases towards 1 as the iteration moves forward. One can also use a bisection search algorithm to identify the best α_ℓ for each iteration [18]. Then, we have

$$\boldsymbol{\theta}_{\ell+1} = \frac{1}{N} \sum_{i=1}^{N} \boldsymbol{\theta}_{\ell+1}^{(i)}. \tag{27}$$

The iteration procedure repeats itself until convergence when the difference in two consecutive iterations is less than a prespecified tolerance ϵ. This is the ensemble Kalman inversion method. The sampling-based iteration yields approximations of the posterior distribution of the unknown parameters, which can also be viewed as a search within the parameter space. The method is useful in dealing with complex nonlinear relationships from the parameters to the measurements and offers much faster computation than gradient-based optimization when dealing with many complex problems. Algorithm 1 shows a summary of optimal power management based on the method.

Algorithm 1 `EnKI-OPM` Ensemble Kalman inversion-based optimal power management

Set up the optimization problem as in (12)
Convert the problem to a Bayesian parameter estimation problem of $p(\boldsymbol{\theta} \,|\, \boldsymbol{y} = \mathbf{0})$
Initialize by setting $\ell = 0$, $\bar{\boldsymbol{\theta}}_0$, $\boldsymbol{\Sigma}_0^{\boldsymbol{\theta}}$, and $\Delta\boldsymbol{\theta}_0$
Draw samples $\boldsymbol{\theta}_0^{(i)} \sim \mathcal{N}(\bar{\boldsymbol{\theta}}_0, \boldsymbol{\Sigma}_0^{\boldsymbol{\theta}})$, for $i = 1, \ldots, N$
while $\Delta\boldsymbol{\theta}_\ell \geq \epsilon$ **do**
  for $t = k, \ldots, k+H$ **do**
    Generate $\boldsymbol{x}_\ell^{(i)}[t]$ using (23)
    Generate $y_\ell^{(i)}[t]$ as in (24)
  end for
  Construct $\boldsymbol{y}_\ell^{(i)} = \begin{bmatrix} y_\ell^{(i)}[k] & \ldots & y_\ell^{(i)}[k+H] \end{bmatrix}^\top$
  Compute $\bar{\boldsymbol{\theta}}_\ell$ and $\bar{\boldsymbol{y}}_\ell$ via (25a)
  Compute $\boldsymbol{\Sigma}_\ell^{\boldsymbol{\theta}}$, $\boldsymbol{\Sigma}_\ell^{\boldsymbol{y}}$, and $\boldsymbol{\Sigma}_\ell^{\boldsymbol{\theta}\boldsymbol{y}}$ via (25b) - (25d)
  Specify α_ℓ via bisection search
  Update $\boldsymbol{\theta}_{\ell+1}^{(i)}$ via (26)
  Compute $\bar{\boldsymbol{\theta}}_{\ell+1}$ using (27)
  Compute criteria $\Delta\boldsymbol{\theta}_{\ell+1} \leftarrow \|\bar{\boldsymbol{\theta}}_{\ell+1} - \bar{\boldsymbol{\theta}}_\ell\|$
  Set $\ell \leftarrow \ell + 1$
end while
Extract $\hat{\boldsymbol{\theta}}^*[k]$ on convergence
Compute power-sharing ratios $\mu[k]$ using (13)
Apply power-sharing ratios to BESS

TABLE I: Specifications of the BESS

Symbol	Parameter	Value [Unit]
n	Number of battery cells	100
$\bar{Q}$	Cell nominal capacity	2.5 [A.h]
R	Cell internal resistance	30 [mΩ]
R_C	Cell internal resistance	10 [mΩ]
$[q^{\text{min}}, q^{\text{max}}]$	Cell SoC limits	[0.05,0.95]
$[i^{\text{min}}, i^{\text{max}}]$	Cell current limits	[-5,5] [A]
C_{th}	Thermal capacitance	40.23 [J/K]
R_{conv}	Convection thermal resistance	41.05 [K/W]
T_{env}	Environment temperature	298 [K]
Δq	SoC balancing threshold	1%
ΔT	Temperature balancing threshold	0.75 [K]
ϵ	EnKI convergence tolerance	10^{-4}
H	Horizon length	10 [s]

IV. Simulation Results

This section presents the simulation results of the proposed efficient optimal power management on a BESS comprising 100 cells. The key specifications of the considered BESS are summarized in Table I, which are based on the Samsung INR18650-25R cells. The output power profile is designed to periodically charge and discharge the BESS at 1 kW every twenty minutes, as illustrated in Fig. 2. We simulate the BESS operation for one hour with the time steps of one second. We program with Matlab to solve the parameter estimation problem using a workstation with a 3.5 GHz Intel Core i9-10920X CPU and 128 GB of RAM.

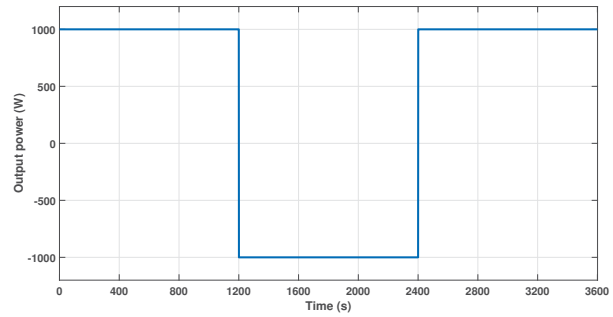

Fig. 2: The output power profile.

For the purpose of implementation, we use a softplus function as the barrier function:

$$\psi(x) = \frac{1}{\alpha} \ln(1 + \exp(\beta x)), \tag{28}$$

where α and β are chosen such that $\psi(x)$ is nearly zero when $x \leq 0$ and takes large numbers when $x > 0$ [19]. Furthermore, β_1 and β_2 in (13) are set to 8 and 12, respectively.

In order to evaluate how well the proposed approach performs, we start by setting the cells' SoC values and internal resistances from uniform distributions $\mathcal{U}(0.7, 0.75)$ and $\mathcal{U}(0.03, 0.04)$ Ω, respectively. The cells' initial temperatures are set to be 298 K. The results obtained from these initializations are presented below.

In Fig. 3, we see the performance of the proposed approach in terms of SoC and temperature balancing. For better interpretation, we also present the estimated parameters in Fig. 4. The simulation starts with an uneven distribution of SoC across the cells. We observe in Fig. 4 that the proposed approach initially prioritizes SoC balancing by setting θ_1 close to one. This results in the ensuing convergence of the cells' SoC values, as shown in Figs. 3 (a), (b). However, the cells' temperatures start to drift away from each other, and at about 300 seconds, the deviation in temperatures reaches the maximum allowed threshold (see Figs. 3 (c), (d)). At this point, the approach reduces θ_1 and increases θ_2 to maintain the cells' temperature within the desired range, as illustrated in Fig. 4.

Moving forward, after around 750 seconds of the simulation, it is no longer possible to maintain both SoC and temperature balanced. This behavior is a consequence of the infeasibility of the underlying optimization problem, where achieving both SoC and temperature balancing is not feasible. As a result, a slight deviation of the cells' SoC is allowed to keep the cells' temperature within the desired

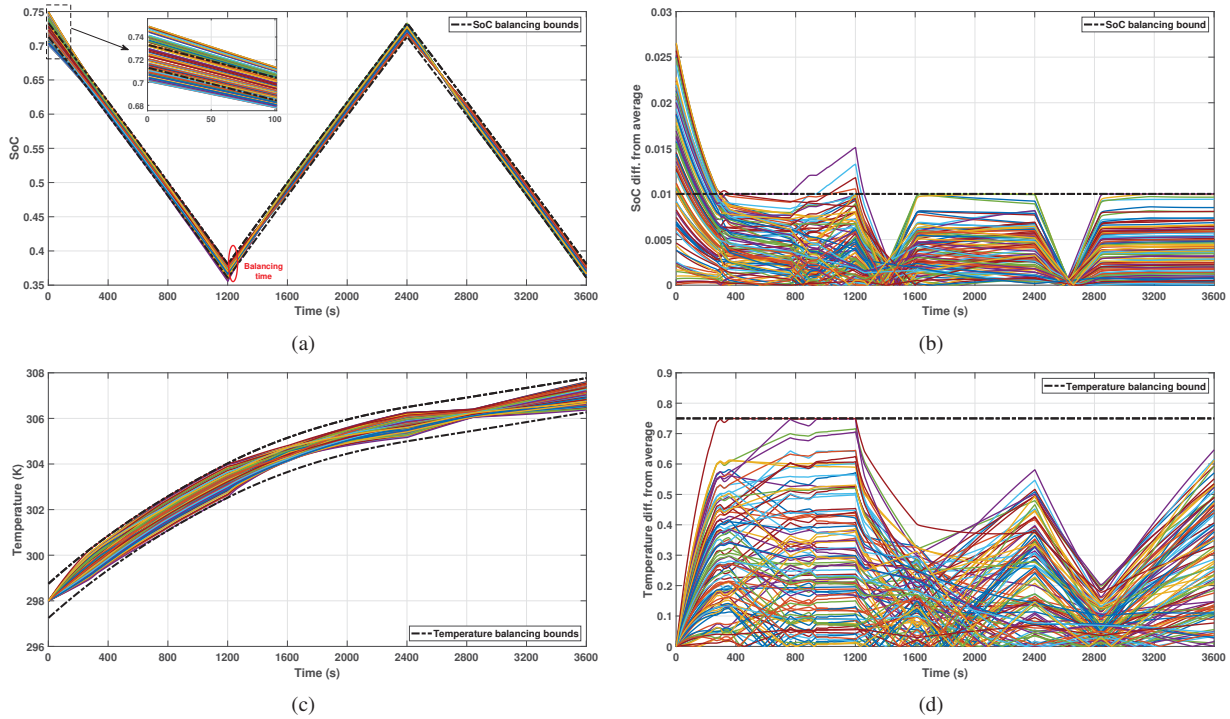

Fig. 3: Simulation results of the SoC and temperature balancing. (a) The SoC of the cells. (b) The deviation of the cells' SoC from the average. (c) The temperature of the cells. (d) The deviation of the cells' temperature from the average.

bound. This behavior continues until the charging cycle starts for the BESS at the 1200-th second.

The charging cycle allows the proposed approach to attain SoC and temperature balancing simultaneously. Looking at Fig. 4, we observe that the proposed approach increases θ_1. At roughly the 1300-th second, the cells are balanced, and the proposed approach maintains the balance from thereon. After ensuring that both the SoC and temperature are balanced, the proposed approach focuses on minimizing the power losses by reducing θ_1 and θ_2 after the 1300-second mark. During this period, the BESS operation allocates the output power demand among the cells based on their internal resistances to achieve the power-loss-minimized operation. This period lasts until the 1600-second mark, when the SoC balancing constraint is activated (as shown in Fig. 3 (b)). After this point, the proposed approach increases θ_1 and θ_2 and continues to minimize power losses while also maintaining balanced SoC and temperature among the cells.

At the time instant of 2400 seconds, the BESS transitions to a discharging cycle. This shift allows the proposed approach to enforce power loss minimization while adhering to the SoC and temperature balancing constraints. As a result, θ_1 and θ_2 are decreased, as shown in Fig. 4. However, the SoC values of the cells diverge until they reach the SoC balancing threshold at around the 2850-th second. At this point, the proposed approach increases θ_1 and θ_2 to keep the cells within the desired balancing bounds.

Fig. 4 shows the parameters of the designed control policy,

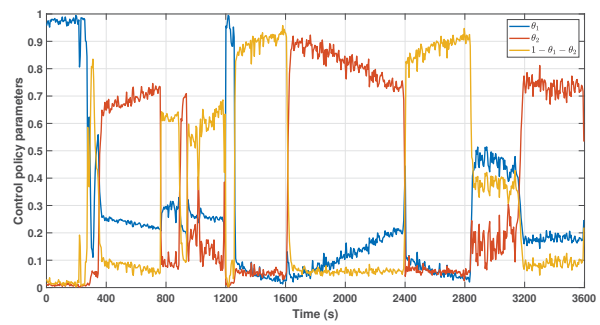

Fig. 4: The estimated parameters of the control policy.

and based on these parameters, we use (13) to calculate the power-sharing ratios of the cells, which are illustrated in Fig. 5. These power-sharing ratios are used to distribute the output power demand among the cells. This differentiation aims to minimize the power losses while ensuring that the SoC and temperature of each cell are balanced. It is essential to observe that when the cells are almost balanced (e.g., during the time interval of 2900$\sim$3600 seconds), the power-sharing ratios converge towards $1/n$, requiring only minor adjustments to maintain the balancing condition.

The objective of our proposed approach is to deliver a computationally efficient solution for the optimal power management of large-scale BESS. Table II presents the average computation times associated with our approach, considering different cell numbers and ensemble sizes for the EnKI.

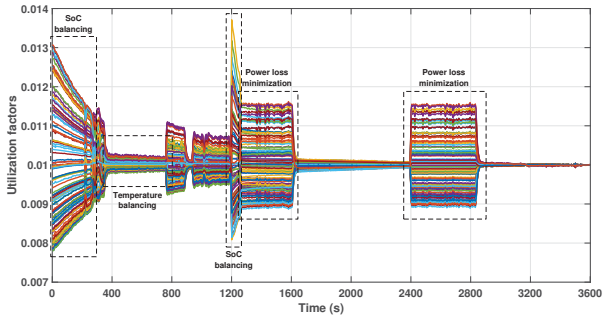

Fig. 5: The evolution of the cells' power-sharing ratios.

TABLE II: Computation times of the proposed approach.

Ensemble size	Number of cells		
	20	50	100
EnKI-50	0.79 s	1.33 s	3.29 s
EnKI-100	0.99 s	1.89 s	6.24 s
EnKI-200	1.57 s	2.89 s	6.37 s

Our results demonstrate that the computation time for our proposed approach consistently remains below 10-second, even when handling 100 cells. In contrast, gradient-based numerical optimization (12) would typically demand several minutes for just 20 cells and would become impractically burdensome and collapse for 100 cells.

V. Conclusions

As BESS becomes prevalent in various sectors of industry and economy, optimal power management becomes necessary for achieving peak performance. However, optimal power management of large-scale BESS poses significant challenges in terms of computational requirements. To overcome this bottleneck, this paper proposes a computationally efficient approach. We start by introducing power-sharing ratios for the cells, reflecting their corresponding power quota from the output demand. Subsequently, we formulate an optimal power management problem aimed at minimizing power losses, while complying with the safety, balancing, and power conservation constraints. To efficiently solve this problem, we design a parameterized control policy and then recast the optimal power management problem into a parameter estimation task. The ensemble Kalman inversion is employed to perform this parameter estimation. Through extensive simulations, we validate the effectiveness of our proposed approach. Our results demonstrate significant improvements in computation time while maintaining good accuracy.

References

[1] A. Affanni, A. Bellini, G. Franceschini, P. Guglielmi, and C. Tassoni, "Battery choice and management for new-generation electric vehicles," *IEEE Transactions on Industrial Electronics*, vol. 52, no. 5, pp. 1343–1349, 2005.

[2] D. Rosewater and A. Williams, "Analyzing system safety in lithium-ion grid energy storage," *Journal of Power Sources*, vol. 300, pp. 460–471, 2015.

[3] B. Arabsalmanabadi, N. Tashakor, A. Javadi, and K. Al-Haddad, "Charging techniques in lithium-ion battery charger: Review and new solution," in *IECON - 44th Annual Conference of the IEEE Industrial Electronics Society*, 2018, pp. 5731–5738.

[4] J. V. Barreras, C. Pinto, R. de Castro, E. Schaltz, S. J. Andreasen, and R. E. Araújo, "Multi-objective control of balancing systems for li-ion battery packs: A paradigm shift?" in *IEEE Vehicle Power and Propulsion Conference*, 2014, pp. 1–7.

[5] M. Preindl, C. Danielson, and F. Borrelli, "Performance evaluation of battery balancing hardware," in *European Control Conference*, 2013, pp. 4065–4070.

[6] R. Gu, P. Malysz, M. Preindl, H. Yang, and A. Emadi, "Linear programming based design and analysis of battery pack balancing topologies," in *IEEE Transportation Electrification Conference and Expo*, 2015, pp. 1–7.

[7] N. Murgovski, L. Johannesson, and J. Sjöberg, "Convex modeling of energy buffers in power control applications," *IFAC Proceedings Volumes*, vol. 45, no. 30, pp. 92–99, 2012, 3rd IFAC Workshop on Engine and Powertrain Control, Simulation and Modeling.

[8] C. Pinto, J. V. Barreras, E. Schaltz, and R. E. Araújo, "Evaluation of advanced control for Li-ion battery balancing systems using convex optimization," *IEEE Transactions on Sustainable Energy*, vol. 7, no. 4, pp. 1703–1717, 2016.

[9] R. de Castro, C. Pinto, J. Varela Barreras, R. E. Araújo, and D. A. Howey, "Smart and hybrid balancing system: Design, modeling, and experimental demonstration," *IEEE Transactions on Vehicular Technology*, vol. 68, no. 12, pp. 11 449–11 461, 2019.

[10] A. Farakhor, D. Wu, Y. Wang, and H. Fang, "A novel modular, reconfigurable battery energy storage system: Design, control, and experimentation," *IEEE Transactions on Transportation Electrification*, vol. 9, no. 2, pp. 2878–2890, 2023.

[11] R. de Castro, H. Pereira, R. E. Araújo, J. V. Barreras, and H. C. Pangborn, "qTSL: A multilayer control framework for managing capacity, temperature, stress, and losses in hybrid balancing systems," *IEEE Transactions on Control Systems Technology*, pp. 1–16, 2021.

[12] T. Morstyn, M. Momayyezan, B. Hredzak, and V. G. Agelidis, "Distributed control for state-of-charge balancing between the modules of a reconfigurable battery energy storage system," *IEEE Transactions on Power Electronics*, vol. 31, no. 11, pp. 7986–7995, 2016.

[13] Q. Ouyang, J. Chen, J. Zheng, and H. Fang, "Optimal cell-to-cell balancing topology design for serially connected lithium-ion battery packs," *IEEE Transactions on Sustainable Energy*, vol. 9, no. 1, pp. 350–360, 2018.

[14] A. Farakhor, Y. Wang, D. Wu, and H. Fang, "Distributed optimal power management for battery energy storage systems: A novel accelerated tracking admm approach," in *American Control Conference*, 2023, pp. 3106–3112.

[15] H. He, R. Xiong, and J. Fan, "Evaluation of lithium-ion battery equivalent circuit models for state of charge estimation by an experimental approach," *Energies*, vol. 4, no. 4, pp. 582–598, 2011.

[16] N. B. Kovachki and A. M. Stuart, "Ensemble Kalman inversion: a derivative-free technique for machine learning tasks," *Inverse Problems*, vol. 35, no. 9, p. 095005, 2019.

[17] P. L. Houtekamer and F. Zhang, "Review of the ensemble kalman filter for atmospheric data assimilation," *Monthly Weather Review*, vol. 144, no. 12, pp. 4489 – 4532, 2016.

[18] S. Duffield and S. S. Singh, "Ensemble Kalman inversion for general likelihoods," *Statistics & Probability Letters*, vol. 187, p. 109523, 2022.

[19] I. Askari, S. Zeng, and H. Fang, "Nonlinear model predictive control based on constraint-aware particle filtering/smoothing," in *American Control Conference*, 2021, pp. 3532–3537.